Journal of Sound and Vibration (2001) **246**(4), 567–581
doi:10.1006/jsvi.2000.3646, available online at http://www.idealibrary.com on IDEAL®

ON THE JET REGURGITANT MODE OF A RESONANT TUBE

S.-M. Chang and S. Lee

Institute of Advanced Aerospace Technology, School of Mechanical/Aerospace Engineering, College of Engineering, Seoul National University, San 56-1 *Silim-dong, Kwanak-gu, Seoul* 151-742, *Korea. E-mails: smc*1972@*dreamwiz.com; solee@plaza.snu.ac.kr*

(*Received* 18 *August* 2000, *and in final form* 14 *December* 2000)

A conceptual model simplifying the Hartmann–Sprenger tube is suggested and investigated to decouple the regurgitant mode of non-linear physics. In spite of notable difference originating from the complicated flow phenomenon, the resonant behavior of this problem is shown to be dependent primarily on wavelength of resonant wave and depth of the tube. Four main parameters are selected and studied numerically in the present paper: forcing frequency, oscillatory amplitude of the Mach number, distance from oscillatory station to the entry of tube, and tube depth. A resonant motion could be induced by forcing a sinusoidal variation of flow Mach number at the resonance frequency, which supplies vibrational energy to the harmonic system generating compressible waves.

1. INTRODUCTION

The Hartmann–Sprenger tube, installed on the central axis of an underexpanded sonic jet with one end open and the other closed, undergoes a violent vibration with the compression of the tube flow by the impinging jet [1] (see Figure 1a). This resonant tube is being considered for application in to ultrasonic drying, fog dissipation, and the ignition device of a rocket engine, etc. [2]. The vibration energy stored in the tube is emitted resonantly or periodically, and such a resonance induces a pulsatile fluctuation of pressure and temperature at the closed tube wall. However, the Hartmann–Sprenger tube has also been studied from the viewpoint of flow physics, apart from its engineering significance. Since this phenomenon was first reported [3], many researchers in gas dynamics and aero-acoustics society have studied the resonant pulsatile jet noise [4–6]. According to the literature [2], the resonant noise is classified into three main modes: jet instability mode, jet screech mode, and jet regurgitant mode. The first mode is due to the Kelvin–Helmholtz instability generating small toroidal vortices on the slipstream while the second is the high-frequency mode originating from the interaction of the Mach wave and jet boundary.

Although many papers have dealt with the Hartmann–Sprenger tube experimentally and numerically, this problem contains very complex phenomena consisting of the non-linear combination of various modes [1–7]. In a mild (or low pressure) supersonic jet, the jet regurgitant mode is dominant while the jet screech mode becomes important for a strong (or high pressure) jet case [7]. The regurgitant mode, the basic component lying commonly in the mild and the strong pressures, is primarily dependent on the geometrical shape of the tube. According to a linear acoustic theory, the resonant frequencies in a resonant tube, an extreme case of the Hartmann–Sprenger tube, are inversely proportional to the tube depth (see equation (21) of this paper). However, the real physics in a multi-dimensional space shows a far more complicated feature due to the non-linearity of compressible flow. The main question of the present study is how many different much various parametric effects

0022-460X/01/390567 + 15 $35.00/0

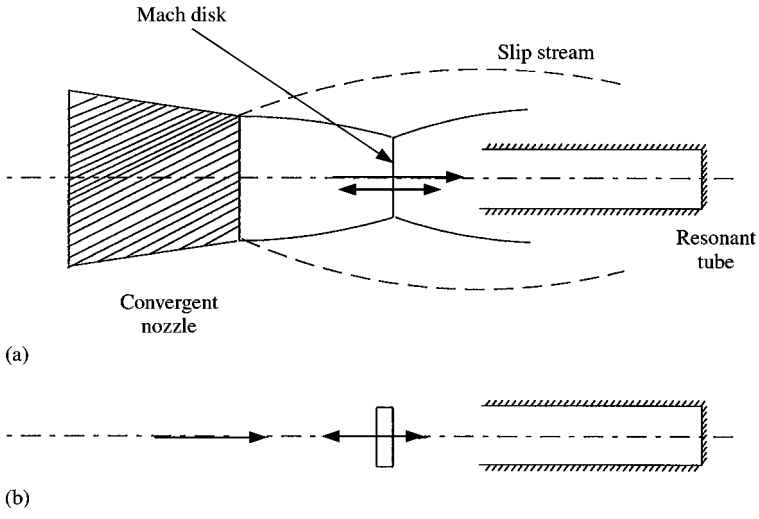

Figure 1. Similarity of the present model to the Hartmann–Sprenger tube: (a) Hartmann–Sprenger tube, (b) Conceptual model.

exist in a resonant process of the closed tube. A new conceptual model simplifying the Hartmann–Sprenger tube is introduced in this paper to separately investigate the jet regurgitant mode. The sinusoidal oscillation at a given frequency (v) is enforced in a compressible flow, and the tube is aligned horizontally along the central axis (see Figure 1b). Axisymmetric Euler equations are solved to obtain flow data, and four main parameters are selected to study their effect on the resonant motion.

2. METHODOLOGY

2.1. DEFINITION OF THE PRESENT PROBLEM

As shown in Figure 2a, the computational domain consists of three components: the inside of the tube, the outside of the tube, and the buffer region to apply the oscillatory boundary condition. The left inlet is vibrated at a given frequency, and the oscillation is propagated to the test region. Three testing points A (forcing station), B (acoustic station), and C (resonant station) for the measure of pressure time history are also marked in Figure 2a. The tube diameter (d) is fixed to 10 mm for the convenience of computation.

Figure 2b is the schematic sketch of the jet regurgitant cycle [1]. When the inlet flow is compressed with the tube wall (Step 1), the compressive wave is radiated at the tube entry producing a reverse-going expansive wave (Step 2) which will be consecutively reflected at the closed tube end (Step 3) and also radiated with a reverse compressive wave (Step 4). However, this cyclic motion will be faded out to the steady state without a source of vibrational energy. If the oscillatory buffer region enforces a proper vibration, it will continue the periodic motion. Our primary interest is the resonance frequency of the regurgitant flow produced by the present system.

2.2. MAIN PARAMETERS

Related variables in the present problem can be listed as follows:

v forcing frequency

a_∞ speed of sound

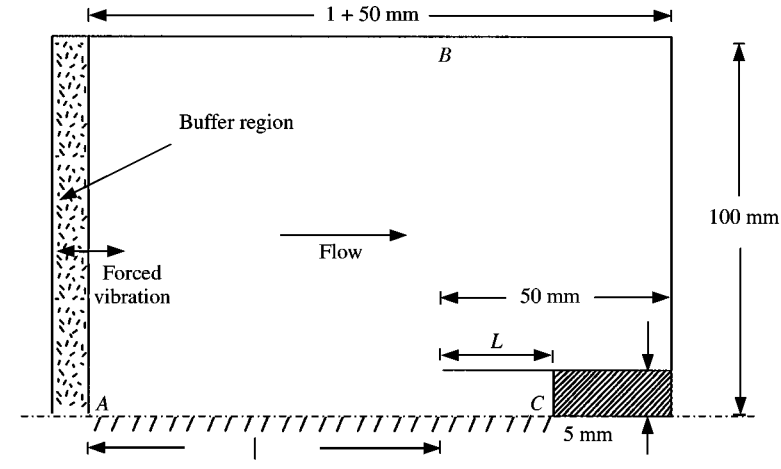

(a)

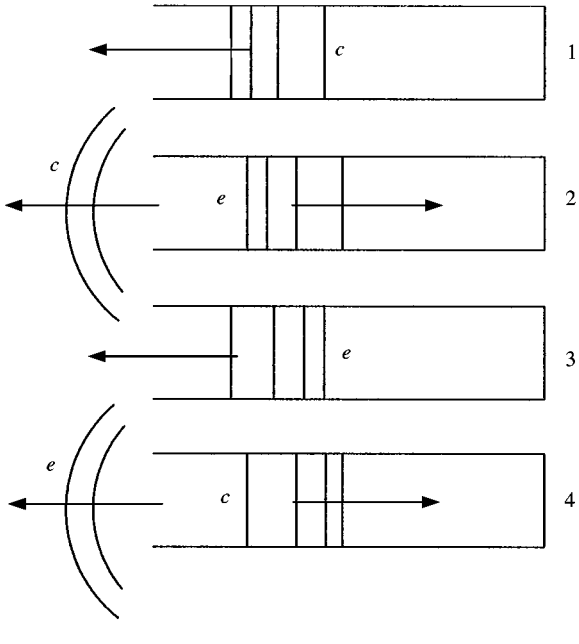

(b)

Figure 2. Basic description on the problem: (a) Definition of the present problem, (b) Schematic sketch for jet regurgitant cycle.

V_∞ flow velocity
l distance between oscillatory position and tube entry
L tube depth
d tube diameter

Applying Buckingham's pi theorem, we obtain four independent dimensionless numbers:

$$\Pi_1 = f_1(V_\infty, L, v) = \frac{Lv}{V_\infty}, \tag{1}$$

$$\Pi_2 = f_2(V_\infty, L, a_\infty) = \frac{V_\infty}{a_\infty} = M_\infty, \tag{2}$$

$$\Pi_3 = f_3(V_\infty, L, l) = \frac{l}{L}, \tag{3}$$

$$\Pi_4 = f_4(V_\infty, L, d) = \frac{L}{d}. \tag{4}$$

The Helmholtz number, K is defined as follows from equations (1), (2), and (4):

$$K = \frac{\omega d}{a_\infty} = 2\pi \Pi_1 \Pi_2 \Pi_4^{-1}, \tag{5}$$

where

$$\omega = 2\pi v.$$

A sinusoidal oscillatory flow field is enforced in the buffer region as mentioned in section 2.1,

$$M(0, t) = M_{mean} + m \sin \omega t. \tag{6}$$

The mean flow Mach number, M_{mean} and the amplitude Mach number, m are subparameters. The other parameters are also defined from equations (3) and (4).

$$D = \frac{l}{L} = \Pi_3, \tag{7}$$

$$S = \frac{L}{d} = \Pi_4, \tag{8}$$

where D is the distance ratio and S is the internal aspect ratio of the tube.

2.3. NUMERICAL STRATEGY

Axisymmetric Euler equations for inviscid compressible flows are written in the following tensor form:

$$\frac{\partial \mathbf{U}}{\partial t} + \frac{\partial \mathbf{F}_j}{\partial x_j} + \mathbf{H} = 0: \quad i, j = 1, 2, \tag{9}$$

where

$$\mathbf{U} = \begin{pmatrix} \rho \\ \rho\, u_t \\ E \end{pmatrix}, \qquad \mathbf{F}_j = \begin{pmatrix} \rho\, u_j \\ \rho\, u_i u_j + p\delta_{ij} \\ u_j(E + p) \end{pmatrix}, \qquad \mathbf{H} = \frac{1}{x_2} \begin{pmatrix} \rho\, u_2 \\ \rho\, u_t u_2 \\ u_2(E + p) \end{pmatrix}$$

and

$$E = \frac{p}{\gamma - 1} + \frac{1}{2} \rho\, u_j u_j.$$

Equation (9) is integrated with finite-volume flux difference method based on the Roe approximate Riemann solver that uses the square-root weight average based on densities of left and right cells to evaluate a numerical flux at the boundary of a given cell. The non-linear right-bounded numerical flux at the cell index j is computed in the following scalar form:

$$f_{j+1/2} = \tfrac{1}{2}(f_j + f_{j+1}) - \tfrac{1}{2}|\lambda_{j+1/2}|(w_{j+1} - w_j), \tag{10}$$

where λ's are eigenvalues of the Jacobian matrix $\partial \mathbf{F}_j/\partial \mathbf{U}$, and w are the conservative variables $\mathbf{U}$ in a diagonally transformed plane. Using equation (10), we spatially integrate equation (9). The temporal integration is formulated in an explicit manner, and the time step is dependent on the eigenvalues and the size of grids by Courant (CFL) condition. However, for a more delicate computation of unsteady flow physics, a higher order is indispensable. The high-order accuracy for space and time is obtained by employing MUSCL algorithm: see details in the textbook of computational fluid dynamics [8]. This scheme is a kind of TVD (total variation diminishing) high-resolution method using a slope limiter, which is applied to remove the dissipation or oscillatory error near the steep waves. Overall, the present numerical scheme reserves the second order accuracy in both space and time: the validation can also be found in reference [7].

The full computational domain is shown in Figure 2a. Flow tangency condition is applied at the tube walls and the symmetric axis (line AC). Along the far boundaries (point B), non-reflecting boundary condition is used, and inlet properties in the buffer region (before the point A) are modified using equation (6). The mass flow is fixed if the inlet flow is choked. Additionally, the momentum is conserved and the adiabatic process across the buffer boundary is assumed:

$$\rho u = \rho_\infty M_{mean} a_\infty, \tag{11}$$

$$\frac{p}{\rho}\{2 + (\gamma - 1)M^2\} = \frac{p_\infty}{\rho_\infty}\{2 + (\gamma - 1)M_{mean}^2\}, \tag{12}$$

$$p(1 + \gamma M^2) = p_\infty(1 + \gamma M_{mean}^2). \tag{13}$$

Therefore, the forcing boundary conditions at the left inlet (point A) in Figure 2a are, from equations (11)–(13),

$$p^-(0, t) = p_\infty \frac{1 + \gamma M_{mean}^2}{1 + \gamma M^2(0, t)}, \tag{14}$$

$$\rho^-(0, t) = \rho_\infty \frac{2 + (\gamma - 1)M^2(0, t)}{1 + \gamma M^2(0, t)} \frac{1 + \gamma M_{mean}^2}{2 + (\gamma - 1)M_{mean}^2}, \tag{15}$$

$$u^-(0, t) = M_{mean} a_\infty \frac{1 + \gamma M^2(0, t)}{2 + (\gamma - 1)M^2(0, t)} \frac{2 + (\gamma - 1)M_{mean}^2}{1 + \gamma M_{mean}^2}, \tag{16}$$

where the superscript, minus sign is introduced in the following sense:

$$p^-(0, t) = \lim_{x \to 0-} p(x, t).$$

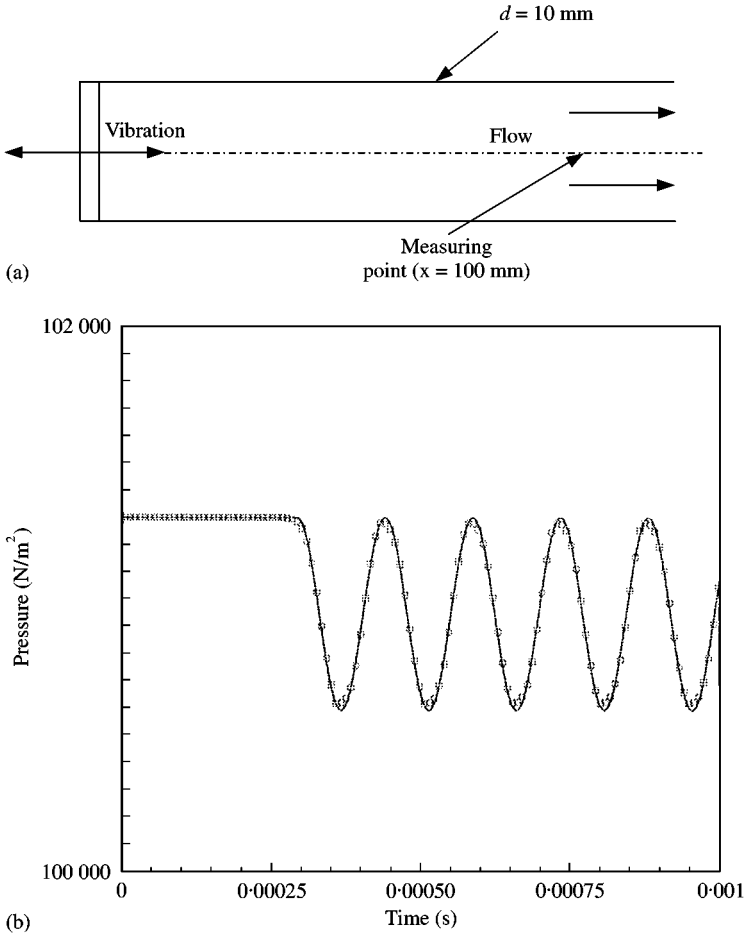

Figure 3. Benchmark problem: (a) Exercise for validation, (b) Pressure history at $x = 100$ mm: ○, analytic solution; ——, numerical result.

2.4. BENCHMARK VALIDATION

The Euler code is briefly validated for a benchmark case of Figure 3a, setting $M_{mean} = 0$ and $v = 3{\cdot}403$ kHz. The acoustic wave is propagated along the pipe as a one-dimensional wave, and the measuring station is located at $x = 100$ mm downstream.

To make a just comparison, we first consider the analytic solution of this benchmark exercise. From equations (6) and (14), the asymptotic series expansion of left boundary pressure becomes

$$p^-(0, t) = p_\infty\{1 - \gamma m^2 \sin^2 \omega t + \gamma^2 m^4 \sin^4 \omega t - \cdots\cdots\}. \tag{17}$$

If small perturbation is assumed, $m \ll 1$, the high-order terms are negligible.

$$p^-(0, t) \approx p_\infty(1 - \gamma m^2 \sin^2 \omega t). \tag{18}$$

The buffer region in Figure 2a and this exercise is not a solid piston since it transmits the inlet flow as well as the surface vibration. Therefore, the Riemann problem must be considered to obtain right boundary values. For the subsonic case,

$$p^-(0, t) = \lim_{x \to 0+} (x, t) = p_\infty(1 - \tfrac{1}{2}\gamma m^2 \sin^2 \omega t). \tag{19}$$

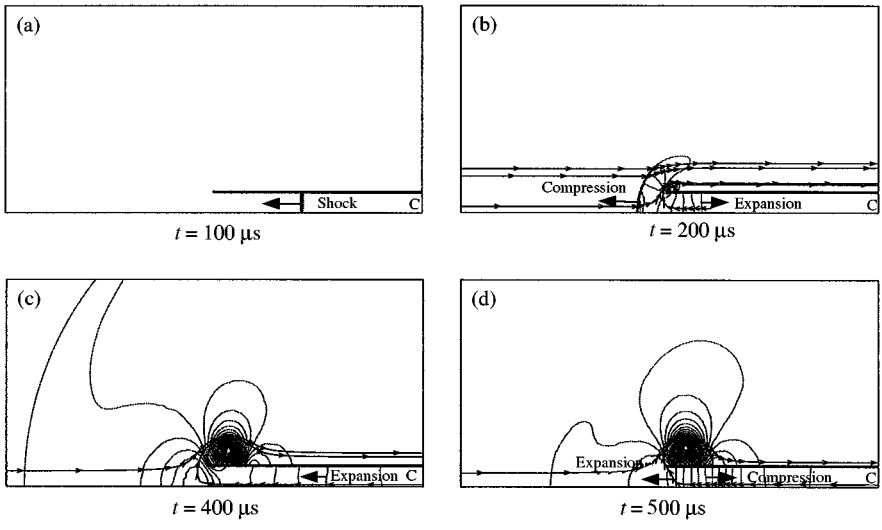

Figure 4. Harmonic motion: pressure contours and streamlines: (a) $t = 100$ μs, (b) $t = 200$ μs, (c) $t = 400$ μs, (d) $t = 500$ μs.

The details of obtaining equation (19) are elucidated in Appendix A of this paper. The acoustic wave is propagated at the speed of a_∞ [9], and the solution is

$$p(x, t) = p_\infty \left\{ 1 - \frac{1}{2} \gamma m^2 \sin^2 \omega \left(t - \frac{x}{a_\infty} \right) \right\}, \tag{20}$$

Figure 3b is the plot of equation (20) compared with the numerical result of the present method. The two data coincide with each other with an extremely trifling error.

From the validation exercise, the dispersive and dissipative errors are shown to be very small at proper frequencies safely below the Nyquist value even for a delicate acoustic propagation problem (refer to Appendix A for details). Hence, we expand the present numerical method directly to the non-linear flow regime.

3. DISTINGUISHING PHYSICS

3.1. HARMONIC MOTION

Under the uniform flow, the end wall of the tube generates compressible waves. Figure 4(a–d) shows sequential isobars and streamlines of the one regurgitant cycle equivalent to Figure 2b, setting $M_{mean} = 0{\cdot}5$, $m = 0$ (no vibration), $D = 2$, and $S = 5$. In Figure 4a, the shock wave propagates to the left (Step 1). When the shock is radiated to the outer field in Figure 4b, the expansive wave is reflected to the right (Step 2). In Figure 4c, the expansion goes to the tube entry after it is reflected from the end wall of the tube (Step 3). Finally the expansive wave is radiated, producing a reverse-going compressive wave: see Figure 4d (Step 4). In all the streamlines in Figure 4(b–d), the regurgitation of flow from the tube is clearly observed.

Figure 5(a–d) shows the pressure histories at positions A, B, C and the Fourier transform of signal C respectively. One cycle of regurgitant mode is marked in Figure 5(a, b), and the farfield acoustic wave contains two peaks of pressure for each period where a peak means

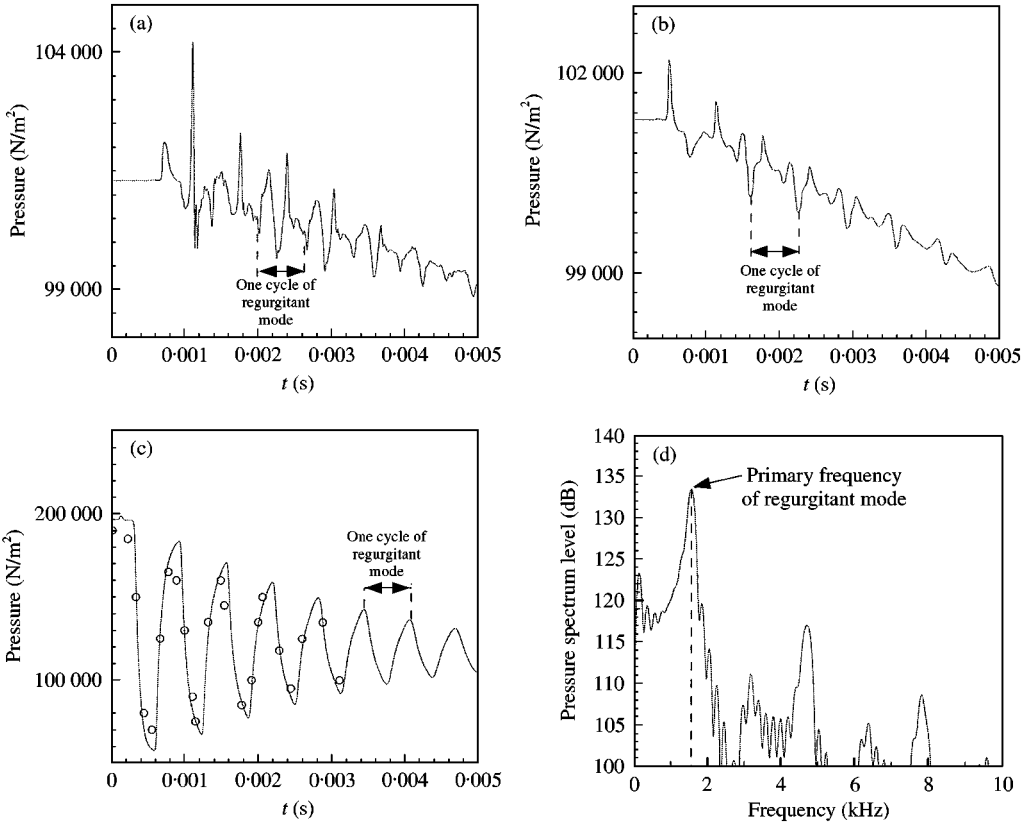

Figure 5. Harmonic motion: $D = 2$ and $S = 5$: (a) Pressure history at point A, (b) Pressure history at point B, (c) Pressure history at point C, ○ Experimental data (Ref. 1), (d) FFT of (c).

a compression–expansion pair. Figure 5c shows that the amplitude of regurgitant mode is decayed to the steady state because no energy is added to this harmonic system. The experimental data in a shock tube experiment [1], marked together in Figure 5c, also coincides with the present numerical simulation. The primary resonance frequency is $v_{res} = 1{\cdot}554$ kHz in Figure 5d. From the one-dimensional acoustic theory, the closed-end organ pipe best transmits acoustic energy at

$$v_{res} = (2n - 1)\frac{a_\infty}{4L}, \tag{21}$$

where n is an integer, and $n = 1$ indicates the primary resonance frequency. The value predicted from equation (21) is $v_{res} = 1{\cdot}702$ kHz (8·80% error), and the discord with the numerical result is due to non-linearity. The inlet flow smoothly turns its direction somewhat ahead of the tube entry and 'the effective tube depth' becomes longer than the original length: check the streamlines of Figure 4(b–d).

3.2. EFFECT OF FORCING FREQUENCY

Two cases are studied for different Helmholtz numbers: $K = 0{\cdot}2$ ($v = 1{\cdot}082$ kHz) and $K = 2$ ($v = 10{\cdot}82$ kHz), setting $M_{mean} = 0{\cdot}5$, $m = 0{\cdot}2$, $D = 2$, and $S = 5$. Figure 6(a–c)

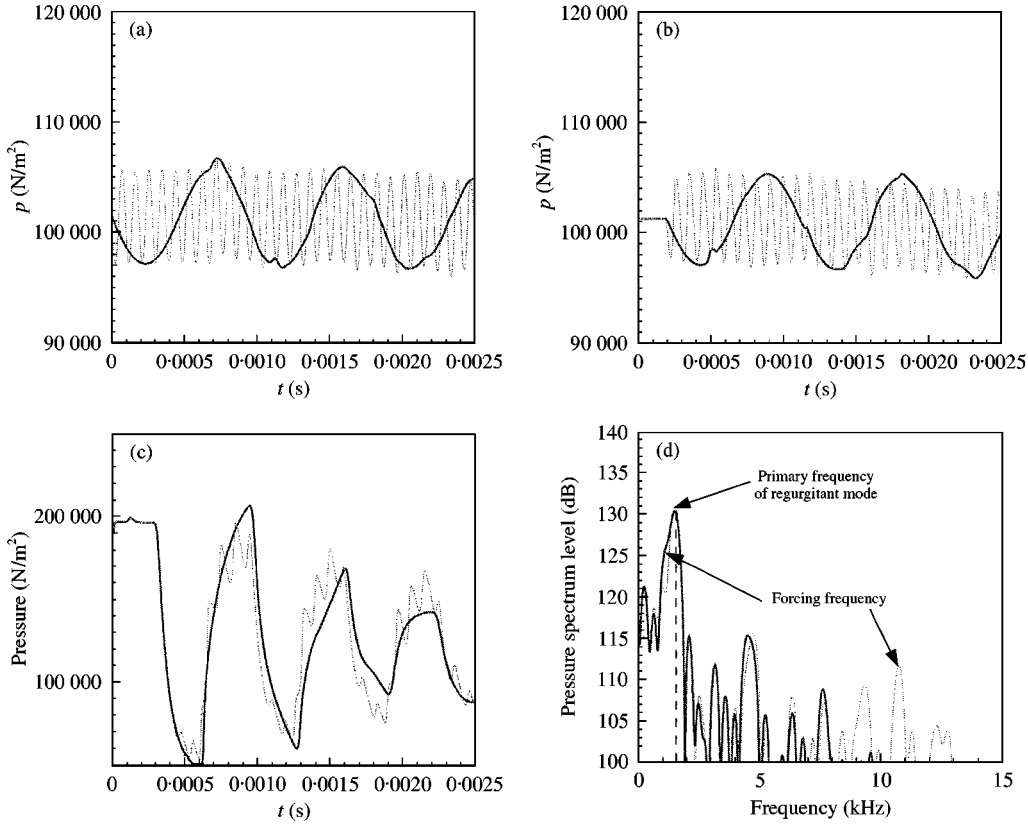

Figure 6. Effect of forcing frequency: $m = 0{\cdot}2$, $D = 2$ and $S = 5$: (a) Pressure history at point A, (b) Pressure history at point B, (c) Pressure history at point C, (d) FFT of (c). ——, 1·082 kHz; — · — · —, 10·82 kHz.

shows pressure histories at points A, B, C, and Figure 6d is the Fourier transform of Figure 6c.

From Figure 6(a, b), it can be pointed out that the forcing motion dominates the whole flow field without remarkable wave deformation. The low-frequency wave enhances only the first cycle of regurgitant mode while the high-frequency wave seems to be maintained for a comparatively long time in Figure 6c. It is due to the fact that the acoustic intensity is proportional to the square of forcing frequency. However, the forcing frequency in these cases cannot significantly change the natural mode shape (see Figure 6d).

3.3. EFFECT OF OSCILLATORY AMPLITUDE OF MACH NUMBER

Three cases are studied for different Mach numbers of the oscillatory amplitude: $m = 0{\cdot}1$, $0{\cdot}2$, and $0{\cdot}4$, setting $v = 1{\cdot}554$ kHz (resonance frequency), $M_{mean} = 0{\cdot}5$, $D = 2$, and $S = 5$. Figure 7(a–c) shows pressure histories at points A, B, C, and Figure 7d is the Fourier transform of Figure 7c.

In Figure 7(a, b), forcing signal at point A and acoustic signal at point B represent wave patterns similar to sinusoidal ones of varying amplitudes. At the resonance frequency, the regurgitant mode is notably enhanced without decaying easily to the steady state (zero amplitude), and the regurgitant motion becomes periodic and pulsatile in Figure 7c.

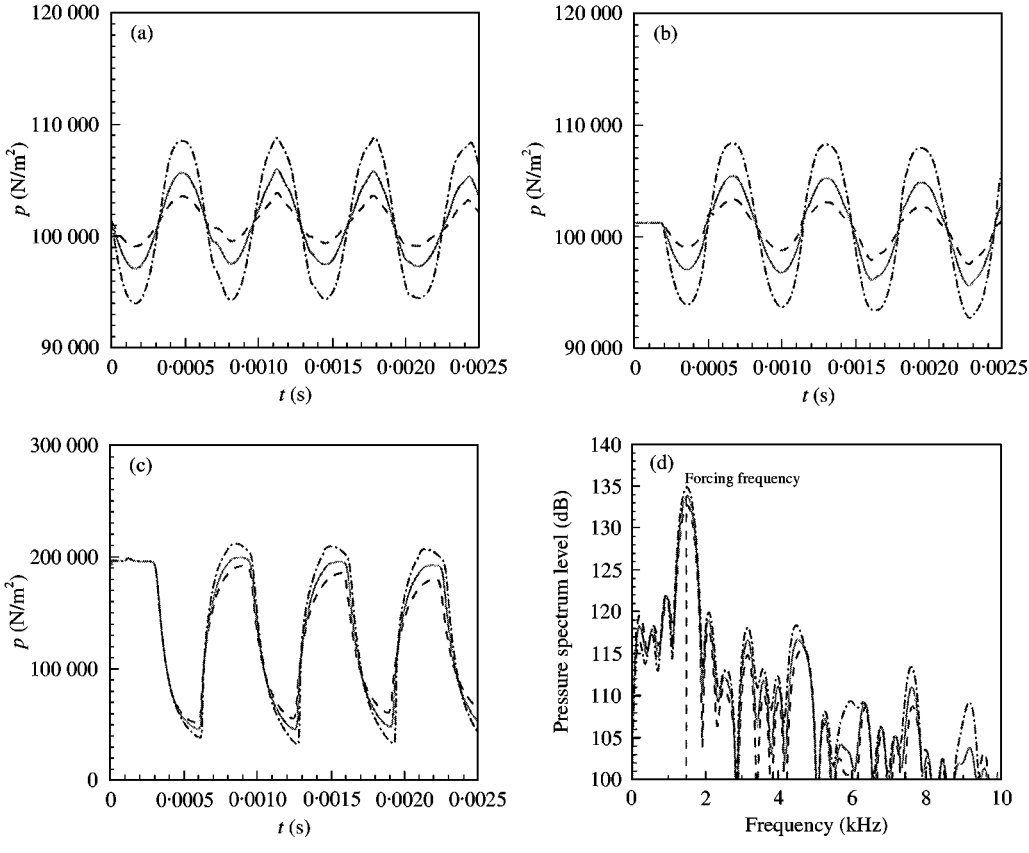

Figure 7. Effect of oscillatory amplitude of Mach number: $D = 2$ and $S = 5$ at resonance frequency: (a) Pressure history at point A, (b) Pressure history at point B, (c) Pressure history at point C, (d) FFT of (c). – – – –, $m = 0{\cdot}1$; ——, $m = 0{\cdot}2$; – · – · –, $m = 0{\cdot}4$.

The damping of regurgitant oscillation observed in the harmonic motion is diminished for the $m = 0{\cdot}1$ case and almost disappears when the amplitude attains $m = 0{\cdot}2$. Moreover, for the $m = 0{\cdot}4$ case, the excessive vibrational energy increases the regurgitant amplitude to a somewhat higher value. The natural mode shape of regurgitation is not significantly changed with various forcing amplitudes (see Figure 7d).

3.4. EFFECT OF DISTANCE BETWEEN OSCILLATORY STATION AND TUBE ENTRY

Three cases are studied for different distances from the oscillatory position to the entry of the tube: $D = 0{\cdot}5$, 1, and 2 ($l = 25$, 50, and 100 mm, respectively), setting $\nu = 1{\cdot}554$ kHz (resonance frequency), $M_{mean} = 0{\cdot}5$, $m = 0{\cdot}2$, and $S = 5$. Figure 8(a–c) shows pressure histories at points A, B, C, and Figure 8d is the Fourier transform of Figure 8c.

The forcing signal at point A is most affected by the regurgitant motion. In Figure 8a, the forcing pressure is severely deformed from the sinusoidal form for the $D = 0{\cdot}5$ and 1 cases. As the settling distance (l) is shorter, the interaction of original wave and regurgitant mode becomes strong. However, this interactive wave component is not propagated to the far field. The acoustic signals at point B recover their original shapes (see Figure 8b). Figure 8c and 8d indicates that the resonant effect is also degraded by regurgitant waves as settling

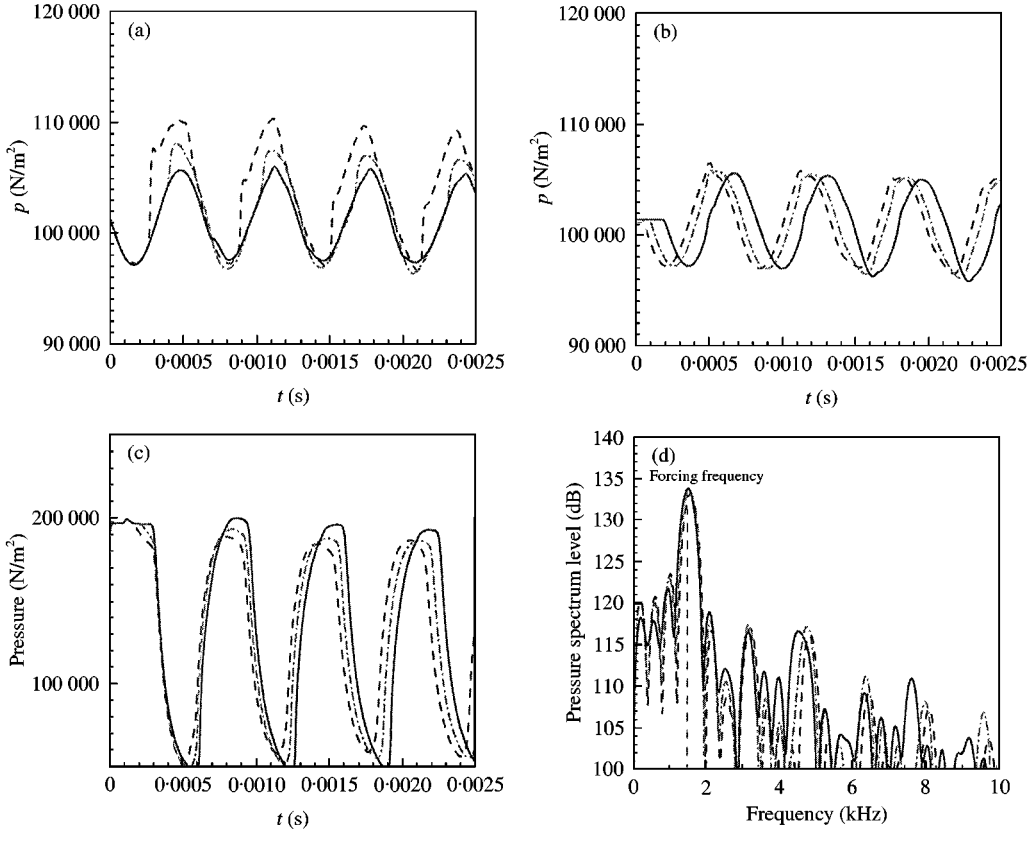

Figure 8. Effect of distance between oscillatory station and tube entry: $m = 0{\cdot}2$ and $S = 5$ at resonance frequency: (a) Pressure history at point A, (b) Pressure history at point B, (c) Pressure history at point C, (d) FFT of (c) – – – –, $l/L = 0{\cdot}5$; – · – · – · –, $l/L = 1{\cdot}0$; ——, $l/L = 2{\cdot}0$.

distance is decreased and the resonance frequency is reduced a little, but these effects are not so significant to be only the second order effect.

3.5. EFFECT OF TUBE DEPTH

Three cases are studied for different depths of the tubes: $S = 0{\cdot}5$, 1 and 5 ($L = 5$, 10, and 50 mm, respectively), setting $v = 1{\cdot}554$ kHz (resonance frequency), $M_{mean} = 0{\cdot}5$, $m = 0{\cdot}2$, and $D = 2$. Figure 9(a–c) are pressure histories at points A, B, C, and Figure 9d is the Fourier transform of Figure 9c.

Obviously the tube depth is the most important factor determining the resonance frequency: recall equation (21). If the forcing frequency is not a resonant one, the regurgitant motion is gradually decayed, but it remains periodic for the third case of resonance frequency in Figure 9c. After the resonant cycle is saturated in the former two cases, the forcing signal dominates in the whole flow field: see Figure 9(a, b) and 9d. In the present problem, the resonance frequency is computed to $v_{res} = 9{\cdot}109$ and $5{\cdot}717$ kHz for $S = 0{\cdot}5$ and 1 cases respectively. Figure 10 is the plot of effective tube depth (L_{eff}) obtained from equation (21) versus the parameter S. A higher S gives a lower value of L_{eff}/L as the deflection of streamlines before the tube entry is less affected with the tube depth. For the

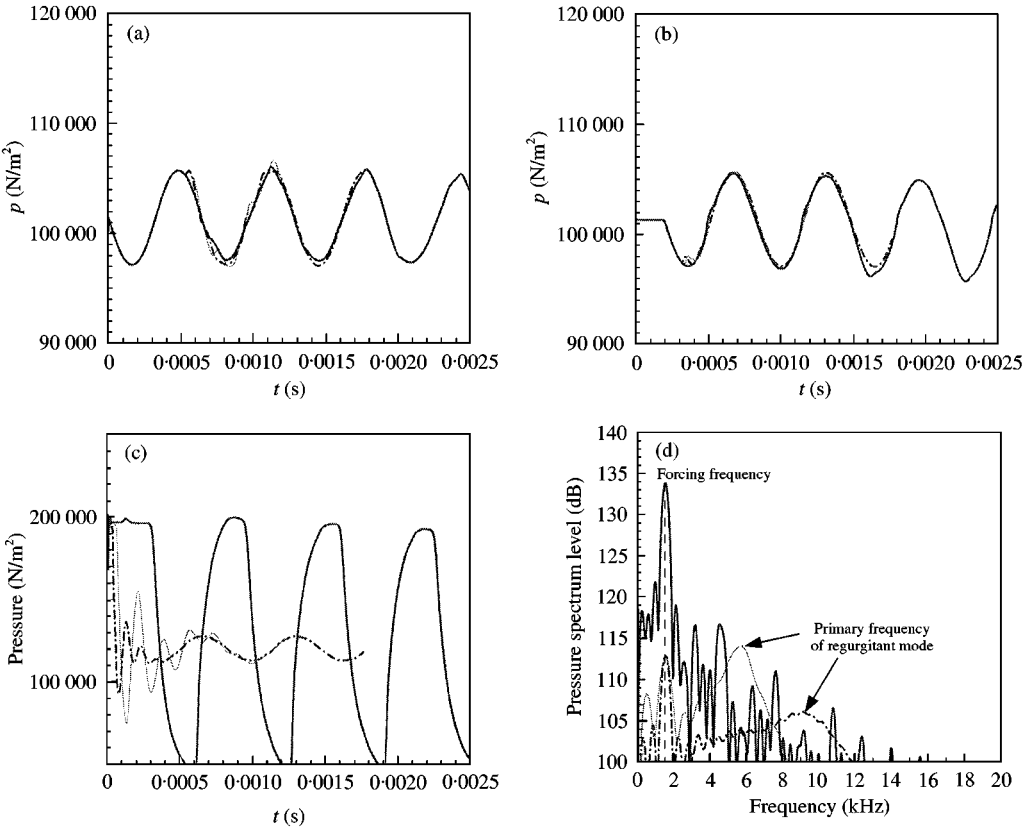

Figure 9. Effect of tube depth: $m = 0{\cdot}2$ and $D = 2$ at resonance frequency of $S = 5$ case: (a) Pressure history at point A, (b) Pressure history at point B, (c) Pressure history at point C, (d) FFT of (c). ·····, $L/d = 0{\cdot}5$; — · — · —, $L/d = 1{\cdot}0$; ———, $L/d = 5{\cdot}0$.

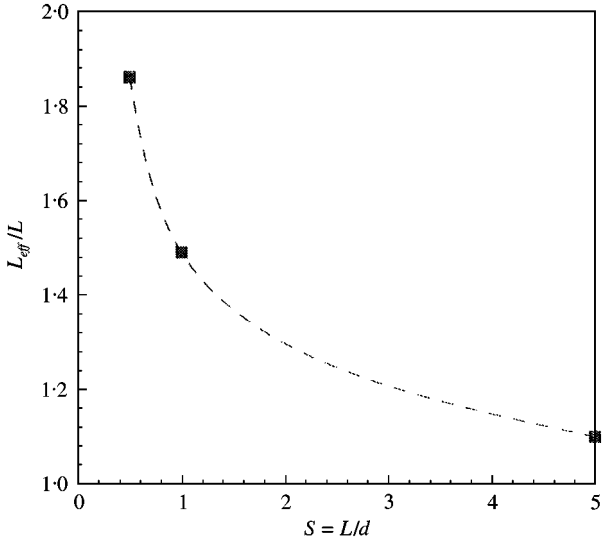

Figure 10. Relation of real and effective tube depth.

long tube $S > 5$, the one-dimensional linear acoustic theory can be approximately used since the error between L_{eff} and L is less than 10%.

4. CONCLUDING REMARK

The present conceptual model has four independent main parameters. They are the Helmholtz number based on the forcing frequency ($K = \omega d/a_\infty$), the flow Mach numbers (M_{mean} and m) , the distance ratio between forcing position and tube entry ($D = l/L$), and the aspect ratio of inner depth of the tube ($S = L/d$). These parameters are studied in the present paper for the fixed mean Mach number, $M_{mean} = 0{\cdot}5$. The boundary condition of oscillatory Mach number, equation (6), is imposed on this system.

Without added oscillation the system is harmonic, and the regurgitant cycle decays in the amplitude as the flow goes to steady state, which is also pointed out in reference [1]. The compressible wave (compression and expansion) can be discerned in pressure contours of Figure 4(a–d): see also the schematic sketch of Figure 2b. When the oscillation tuned to the resonance frequency is enforced, the pressure signal at the tube end shows a resonant pulsatile form because the vibration supplies additional energy to the system. As an overall result, the most important parameter affecting the resonant frequency is the tube depth. However, the distance between the oscillatory position and the tube entry is the secondary parameter determining the regurgitant frequency. As the distance is shorter, its effect becomes larger; it is due to the interaction of the input oscillation and the regurgitant flow. The oscillatory amplitude and the forcing frequency are not so related to the resonant frequency. They only influence is the amount of vibrational energy or the amplitude of resonant pressure signal.

The regurgitant frequency has a little discord with the primary resonance frequency predicted by the one-dimensional acoustic theory, which is due to the streamline deflection ahead of the tube entry causing the longer effective tube depth. As the tube depth is shorter, the non-linearity of compressible flow becomes more significant: see Figure 10. When the aspect ratio, $S = L/d$, is more than 5, the error between the present numerical simulation and the linear theory falls within 10%. Therefore, a short tube contains more non-linearity originating from the compressibility of flow physics.

ACKNOWLEDGMENT

This research is sponsored by the Brain Korea 21 project.

REFERENCES

1. H. D. YANG, S. M. CHANG and K. S. CHANG 1998 *Journal of Korean Society for Aeronautics and Space Science* **26**, 11–19. Impingement of shock wave into a two-dimensional cavity.
2. V. SAROHIA and L. H. BACK 1979 *Journal of Fluid Mechanics* **94**, 649–672. Experimental investigation of flow and heating in a resonance tube.
3. J. HARTMANN 1931 *Philosophical Magazine* **11**, 926–948. On the production of acoustic waves by means of a air-jet of a velocity exceeding that sound.
4. P. A. THOMPSON 1964 *American Institute of Aeronautics and Astronautics Journal* **2**, 1230–1233. Jet-driven resonance tube.
5. G. B. SOBIERAJ and A. P. SZUMOWSK 1986 *Journal of Sound and Vibration* **149**, 375–396. Experimental investigations of an underexpanded jet from a convergent nozzle impinging on a cavity.
6. K. S. CHANG, K. H. KIM and J. IWAMOTO 1996 *International Journal of Turbo and Jet Engines* **13**, 173–182. A study on the Hartmann–Sprenger tube flow driven by a sonic jet.

7. S. M. Ko and K. S. Chang 1998 *Computational Fluid Dynamics Journal* **6**, 439–452. Resonant pulsatile flows of a Harmann–Sprenger tube.
8. S. M. Chang 2000 *Ph.D. Thesis of KAIST*, *DAE*965342. Unsteady shock wave-vortex interactions in the compressible shear layer.
9. A. P. Dowling and J. E. Ffowcs Williams 1983 *Sound and Sources of Sound*. New York: John Wiley & Sons, pp. 19–20.
10. J. D. Anderson 1990 *Modern Compressible Flow*. New York: McGraw-Hill, pp. 237–240.

APPENDIX A: WAVE PROPAGATION IN SUBSONIC AND SUPERSONIC CASES

Figure A.1(a, b) shows pressure signals of the benchmark exercise in Figure 3a.

When the mean flow Mach number (M_{mean}) is changed, the forcing wave pattern induced by the boundary condition of equation (6) and equations (14)–(16) becomes different in subsonic and supersonic cases. The pressure wave is deformed from the sinusoidal shape for mean flow Mach numbers other than 0·5. In Figure A.1a, the phase of pressure signal is changed by 180° in supersonic cases. It is due to the fact expounded in Figure A.1c: the subsonic pressure oscillation is transmitted to the flow field with no phase change, but, when the flow is supersonic, a normal shock wave exists and the wave transmitting it changes the phase.

In Figure Ab, the forcing frequency is varied in the $M_{mean} = 0{\cdot}5$ case. The Nyquist frequency is defined as

$$\nu_{Nyquist} = \frac{a_\infty}{2\Delta x} \tag{A1}$$

which is 170·2 kHz for this problem. However, the computational dissipation requires the narrower band to perform a valid computation. The propagating signal is diminished even for the case of $\nu = \nu_{Nyquist}/10 = 17{\cdot}02$ kHz. Therefore, the application of the Euler code is restricted to only low-frequency oscillations in the present study.

The Mach number is oscillated in the sinusoidal form like equation (6), and the pressure is varied with equation (14) at the buffer zone in Figure 2a. If $M_{mean} = 0$, the pressure signal is propagated as an acoustic wave. From equation (14), the left boundary condition of pressure is expressed as equation (18) with the small-perturbation approximation. However, this boundary value is not directly propagated to the downstream flow, and the Riemann problem must be solved to obtain the right boundary value (see Figure A.1d depicting Riemann waves such as shock wave, contact discontinuity, and rarefaction wave). From a reference literature [10], the exact relation between the right (superscript +) and the left (superscript −) pressure in the shock tube problem is

$$p^- = p^+ \left\{1 - \frac{(\gamma - 1)(p^+/p_\infty - 1)}{\sqrt{2\gamma[2\gamma + (\gamma + 1)(p^+/p_\infty - 1)]}}\right\}^{-2\gamma/(\gamma - 1)}, \tag{A2}$$

where the left value p^- is known. If we assume that the right value is in the following form:

$$p^+(0, t) = p_\infty(1 - k\gamma m^2 \sin^2 \omega t) \tag{A3}$$

substituting (A3) into (A2), and for the small m,

$$p^- = p^+\left\{1 + \frac{(\gamma - 1)k\gamma m^2 \sin^2 \omega t}{2\gamma\sqrt{1 - 0{\cdot}5(\gamma + 1)km^2 \sin^2 \omega t}}\right\}^{-2\gamma/(\gamma - 1)} \approx p^+(1 - k\gamma m^2 \sin^2 \omega t).$$

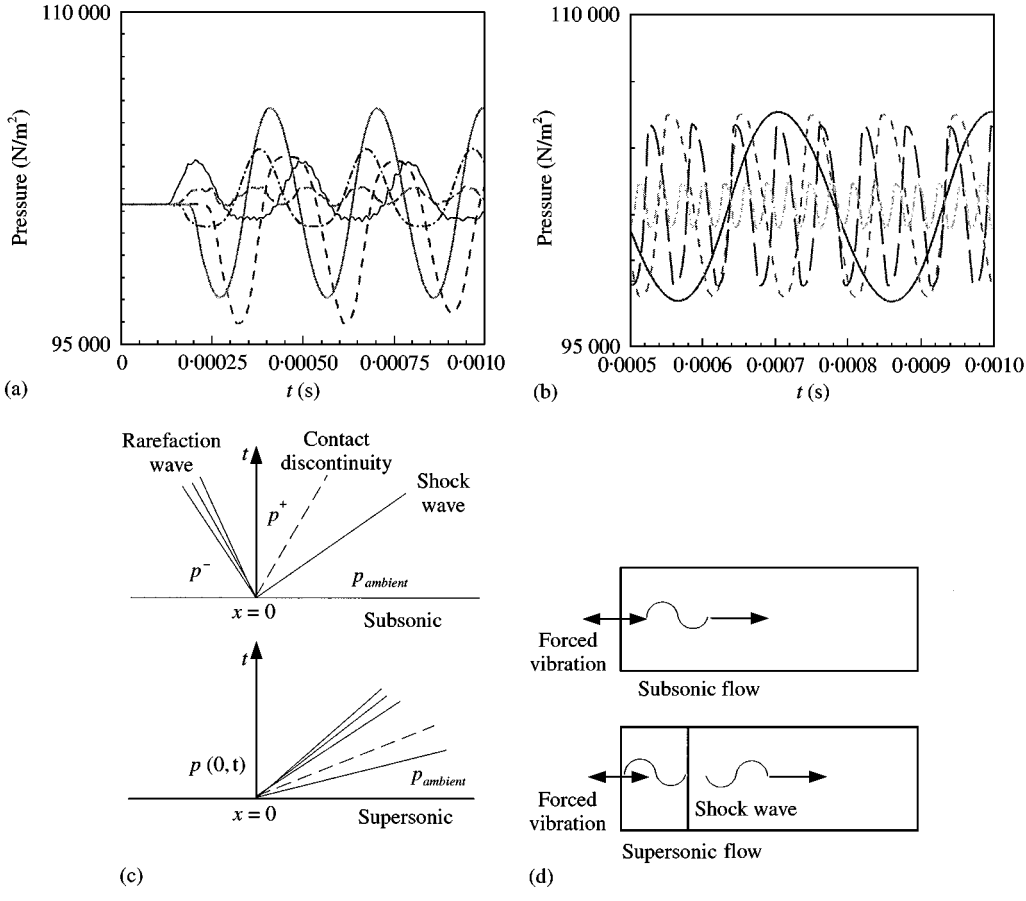

Figure A1. Subsonic and supersonic wave propagation: (a) Effect of mean flow Mach number: – – – –, $M_{mean} = 0{\cdot}2$; ——, $M_{mean} = 0{\cdot}5$; ——, $M_{mean} = 0{\cdot}8$; – – – –, $M_{mean} = 1{\cdot}0$; ——, $M_{mean} = 1{\cdot}2$, (b) Dissipation of acoustic wave for the given forcing frequency: ——, 3·403 kHz; – – – –, 10·209 kHz; — —, 17·015 kHz; ——, 34·03 kHz, (c) Subsonic and supersonic boundary conditions, (d) Schematic diagram of acoustic wave propagation.

From equations (18) and (A3), the above is simplified to

$$k \approx \tfrac{1}{2}. \tag{A4}$$

Therefore, equation (19) is derived. This Riemann solution is required only for subsonic flow, and $p(0, t) = p^+ = p^-$ for supersonic cases as shown in Figure A.1d.